Contents

Part I

ActiveAx

Chapter 1

In-vivo estimates of axonal characteristics using the single fibre protocols

1.1 Introduction

In the previous chapter we have introduced the single fibre $\mathcal{SF}$ diffusion MRI protocol optimisation framework designed for unidirectional white matter tracts. The aim of this chapter is to investigate the clinical feasibility of the $\mathcal{SF}$ protocols to estimate axon diameter and axon density indices in-vivo. (Alexander et al., 2010) has already shown that such indices can be acquired in-vivo on a standard clinical system, but the long scan time of 1 hour is permissive for routine clinical application. We have shown in simulations that $\mathcal{SF}$ protocols allow more accurate estimates of microstrucure indices in such structures compared to the orientational invariant $\mathcal{OI}$ approach of (Alexander, 2008). We further demonstrated the feasibility of estimating a biologically reasonable range of axon diameter and axon density indices in a sample of fixed primate spinal cord. Our initial results suggest that $\mathcal{SF}$ protocols can produce acceptable estimates of tissue microstrucure indices using a only a moderate number of diffusion weighted acquisitions.

Our aim is to produce a $\mathcal{SF}$ protocol that can be acquired within 25 minutes, which is comparable scan time to a typical DTI protocol. We achieve this by reducing the total number of diffusion weighted directions ($\mathcal{SF}$) compared to Alexanders's original 1 hour $\mathcal{OI}_{360}$ approach. We first compare Monte-Carlo simulations of the $\mathcal{SF}$ protocol with with the $\mathcal{OI}$ approach. We then evaluate both methods in an MRI scan/rescan experiment on two healthy volunteers to investigate the feasibility of estimating microstructural parameters in-vivo under realisitic clinical conditions.

1.2 Asymptotic protocol optimisation

In the previous chapter we have implemented a $\mathcal{SF}$ protocol optimisation, given a total number of acquisitions N divided in M sets of different pulsed gradient
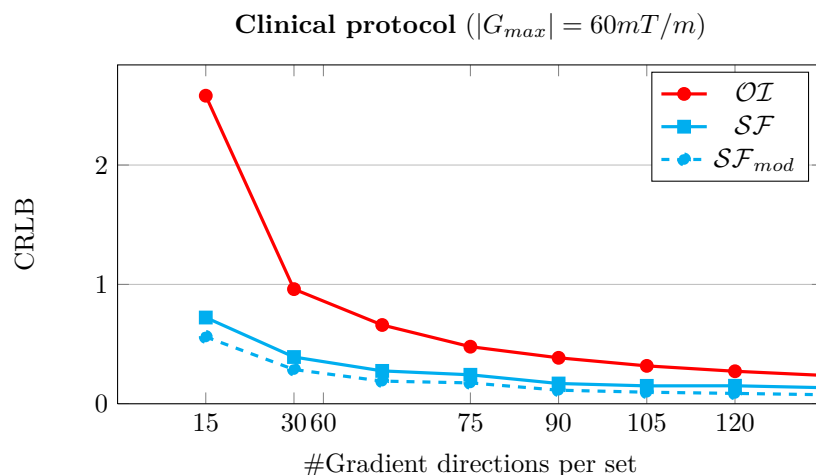
Clinical protocol $(|G_{max}| = 60mT/m)$

Figure 1.1: Comparision of CRLBs between $\mathcal{OI}$, $\mathcal{SF}$ and the modified $\mathcal{SF}_{mod}$ protocols for different number N of gradient directions per set.

spin echo (PGSE) pulse settings with the gradient scheme being either fixed $\mathcal{OI}$ or optimised for each set $\mathcal{SF}$. Our simulations showed that protocols with optimised gradient schemes consistently outperformed the protocols with a fixed uniform gradient scheme. While the complete optimisation of all gradient directions offers great flexibility, but is also very computationally demanding. The increase in free parameters increases the computational complexity and thus requires much longer computation times compared to $\mathcal{OI}$. The larger parameter space also causes a higher risk for the algorithm to converge to local minima instead of the global minimum.

We observed in the previous chapter that the $\mathcal{SF}$-optimised gradient schemes converged to a trivial arrangement of gradient directions, featuring predominantly perpendicular and parallel measurements to the given fibre direction. In fact, we can hypothesise that the few variations in gradient direction do not reflect the true optimal gradient scheme, but are caused by imperfections in the optimisation algorithm. To test this hypothesis, we can simply use the $\mathcal{SF}$ presented e.g. in the previous chapter to produce a modified $\mathcal{SF}_{mod}$ protocol with only parallel and perpendicular gradients by aligning each gradient to the closest perpendicular or parallel gradient direction. Figure 1.1 compares the CRLB values for such a modified $\mathcal{SF}_{mod}$ protocol compared to the untouched $\mathcal{SF}$ and $\mathcal{OI}$ protocols for different numbers of gradient directions. Not only does the $\mathcal{SF}_{mod}$ protocol achieve a similar improvement of CRLB values to $\mathcal{SF}$ over the $\mathcal{OI}$ method, but it even gives the smallest CRLB values out of the three methods. This suggests that it is sufficient to acquire only in parallel and perpendicular directions.

To reduce the complexity of the optimisation problem we therefore constrain our measurements in the protocol to have gradient directions only perpendicular to the fibre bundles, but we include one measurement in the parallel direction for the estimation of diffusivity along the axons. Such gradient scheme contains exclusively either parallel or perpendicular measurements, and thus can be considered independent of the number of gradient directions N in each set

M. We can therefore replace the optimisation for each pair of (N, M), with an asymptotic optimisation for $N \to \infty$ (in the following referred to as $\dashv\mathcal{SF}$). The $\dashv\mathcal{SF}$ approach allows us to introduce the weighting factors w_m that reflect how important each measurement is, i.e. how often it should be sampled relative to the other measurements. We can then adapt Eq. **??** so that:

$$\Omega = diag\{w_1, \cdots, w_M\} \text{ with } \sum_{m=1}^{M} w_m = 1 \tag{1.1}$$

For any given desired number of measurements the discrete number N of measurements per set can be simply calculated by $N_m = w_m N$. Table **??** summarises the optimisation parameters for the asymptotic protocol optimisation in comparision with the $\mathcal{OI}$ and $\mathcal{SF}$ methods described in the last chapter. Please note that the computational complexity of the $\dashv\mathcal{SF}$ is only dependent on M, making it similar to the complexity of $\mathcal{OI}$ and significantly less demanding than $\mathcal{SF}$.

Table 1.1: Overview of parameters for the tested protocol optimisation approaches.

	$\dashv\mathcal{SF}$	$\mathcal{OI}$	$\mathcal{SF}$
Free parameters	$w_m, \delta_m, \Delta_m, G_m$	δ_m, Δ_m, G_m	$\phi_{m,n}, \theta_{m,n}, \delta_m, \Delta_m, G_m$
Fixed parameters	ϕ_n, θ_n	ϕ_n, θ_n	–
Specific fibre direction	yes	no	yes
No. of free parameters	O(M)	O(M)	O($M \times N$)

1.3 Experiments & Methods

.....

Protocols

We generate optimized protocols for our 3T Philips Achieva scanner with a maximum diffusion gradient strength ($|G|$) strength of $|\vec{G}_{max}| = 60mT/m$. $\dashv\mathcal{SF}$ optimization is performed for the same two-compartment tissue model and parameter range we described in the previous chapter. The asymptotic $\dashv\mathcal{SF}$ protocol optmisation is performed and we derive a protocol with a total of 90 diffusion weighted acquisitions ($\mathcal{SF}_{90}$), which corresponds to the desired 25 minutes of scan time on our scanner. For comparison, we also generate an $\mathcal{OI}$ protocol $N = 360$ ($\mathcal{OI}_{360}$) as used in (Alexander et al., 2010) and an $\dashv\mathcal{SF}$ protocol with the same number of acquisitions ($\mathcal{SF}_{360}$). The three protocols are presented in table 1.2. For the $\mathcal{SF}_{90}$ and $\mathcal{SF}_{360}$ protocols we used $M = 8$ but only sequences with $w > 0$ are reported. The $\mathcal{OI}_{360}$ protocol optimisation uses $M = 4$ and report the three unique PGSE parameter settings.

Table 1.2: PGSE settings of $\mathcal{SF}_{90}$, $\mathcal{SF}_{360}$ and $\mathcal{OI}_{360}$ protocols. $\perp$ and $\parallel$ mark acquisitions perpendicular and parallel to the fibre bundles.

(a) $\mathcal{SF}_{360}$ and $\mathcal{SF}_{90}$ protocols

N_m	Δ [ms]	δ [ms]	G [mT/m]	b [s/mm²]	
70	18	0	0	0	0	
72	17	33.0	14.5	36.8	550	$\parallel$
38	10	22.4	15.9	60.0	1114	$\perp$
45	11	29.3	22.8	60.0	2908	$\perp$
68	17	48.0	26.6	43.7	3666	$\perp$
67	17	40.5	34.0	60.0	8692	$\perp$
360	90					

(b) $\mathcal{OI}_{360}$ protocol

N_m	Δ [ms]	δ [ms]	G [mT/m]	b [s/mm²]
71	0	0	0	0
101	19.2	11.7	60.0	540
107	38.2	12.5	47.8	870
81	29.1	21.6	60.0	2634
360				

Simulations

We use the free diffusion simulation of **?**, which performs a Monte Carlo (MC) simulation of water particles in packed cylinders. We use the 44 synthetic white matter substrates fromAlexander et al. (2010) with diameter distributions and packing densities similar to previously reported histology studies (**???**).We perform the MC simulation with 50000 walkers and 20000 time steps for each protocol. For each substrate we generate 10 sets of noise-free MR signals and add Rician noise of $\sigma = 0.05$, resulting in total of 440 sets of noisy MR signals. For each protocol we apply the model fitting procedure to the 440 sets of MR signals and retrieve the tissue model parameters.

To compare the axon distributions with the estimated axon diameter index a we have to take into consideration that the contribution of each axon to the MR signal depends its volume and is proportional to the square of its diameter. As in Alexander et al. (2010) we correlate the estimated axon diameter index a with the weighted axon diameter average $\hat{a} = \hat{f}/\int p(\alpha)\alpha^3 d\alpha$, where p is the true distribution of axon diameter α and $\hat{f}$ is the intracellular volume fraction $\hat{f} = \int p(\alpha)\alpha^2 d\alpha$.

MRI experiment

The $\mathcal{SF}_{90}$ and $\mathcal{OI}_{360}$ protocols (see table 1.2) are implemented on our 3T Philips Achieva scanner to test the clinical viability of the 25 minute $\mathcal{SF}_{90}$ protocol and compare it to the three times longer $\mathcal{OI}_{360}$ protocol. Diffusion weighted

MR images of two healthy volunteers (male 32yo, female 25yo) are acquired using a cardiac-gated EPI sequence with imaging parameters similar to the protocol described in (Alexander et al., 2010): 8 channel Philips head-coil, 10 slices, slice thickness=5mm, in-plane resolution=128x128 (FOV=35x35mm^2), TR=7RR, TE=125ms/TE=100ms for $\mathcal{SF}_{90}$ and $\mathcal{OI}_{360}$ respectively. We position the centre slice so that it is aligned with the mid-sagittal body of the corpus callosum (CC) to be able to acquire DWI measurements perpendicular and parallel to the fibres of the CC. $\mathcal{SF}_{90}$ acquisition is repeated twice on two separate days for each subject to investigate the reproducibility of the estimated parameter maps.

Model fitting

We use the three stage fitting algorithm as described in Alexander et al. (2010), to fit the tissue model to the MR signal in each voxel. We increase stability by fixing $d_\parallel$ to $1.7 \cdot 10^{-9} m^2 s^{-1}$ and d_I is fixed to $3.0 \cdot 10^{-9} m^2 s^{-1}$ (Assaf et al., 2008; Barazany et al., 2009; Alexander et al., 2010). The objective function is defined as the maximum likelihood of model parameters given the observed MR signals under Rician noise ($\sigma = 0.05$). An initial estimation is found using a coarse grid search algorithm over a set of physiologically possible parameters. Then a gradient descent algorithm further refines the parameter estimates. Finally a Markov Chain Monte Carlo (MCMC) algorithm with a burn-in of 2000, 50 samples at an interval of 200 provides posterior distributions of the parameters f_1, f_2 and the axon radius r. An average over the MCMC samples provides the final parameter estimates. We report the axon diameter index $a = 2r$ and the axon density index $\rho = 4f_1\pi^{-1}r^{-2}$.

1.4   Results

Simulations

Figure 1.2 presents the results from fitting the model to the synthetic MC data sets as described above. For all three protocols we plot the fitted axon diameter index a against $\hat{a}$ and the intra-cellular volume fraction f_1 against the true intra-cellular volume fraction $\hat{f}$ for all 440 noisy sets of MR signals. We also compute the mean over the 10 replications for each of the 44 unique substrates and display them in the same plot. The bottom row of Fig.1.2 shows that all protocols estimated the volume fraction accurately with little variance. Further, all protocols estimate larger a that agree with $\hat{a}$. The estimated a varies arbitrarily between $0 - 2\mu m$ for $\hat{a} < 3\mu m$. Thus smaller $\hat{a}$ can be distinguished from larger ones but not accurately measured. This is because the limited maximum $|G|$ that does not attenuate the signal from water inside axons of diameter $< 2\mu m$. Despite the limitation, the trends of a agree with the true values for $\hat{a}$ and suggest that the index a is a useful discriminator of axon diameter distributions. $\mathcal{SF}_{360}$ estimates both indices more accurately than $\mathcal{OI}_{360}$ and variations among the 10 estimates in each substrate are smaller. $\mathcal{SF}_{90}$ and $\mathcal{OI}_{360}$ appear to have similiar accuracy and precision in estimating $\hat{a}$ and $\hat{f}$. This suggests that we can reduce by a third by exploiting a-priori known fibre orientation while maintaining similar quality of parameter estimates.
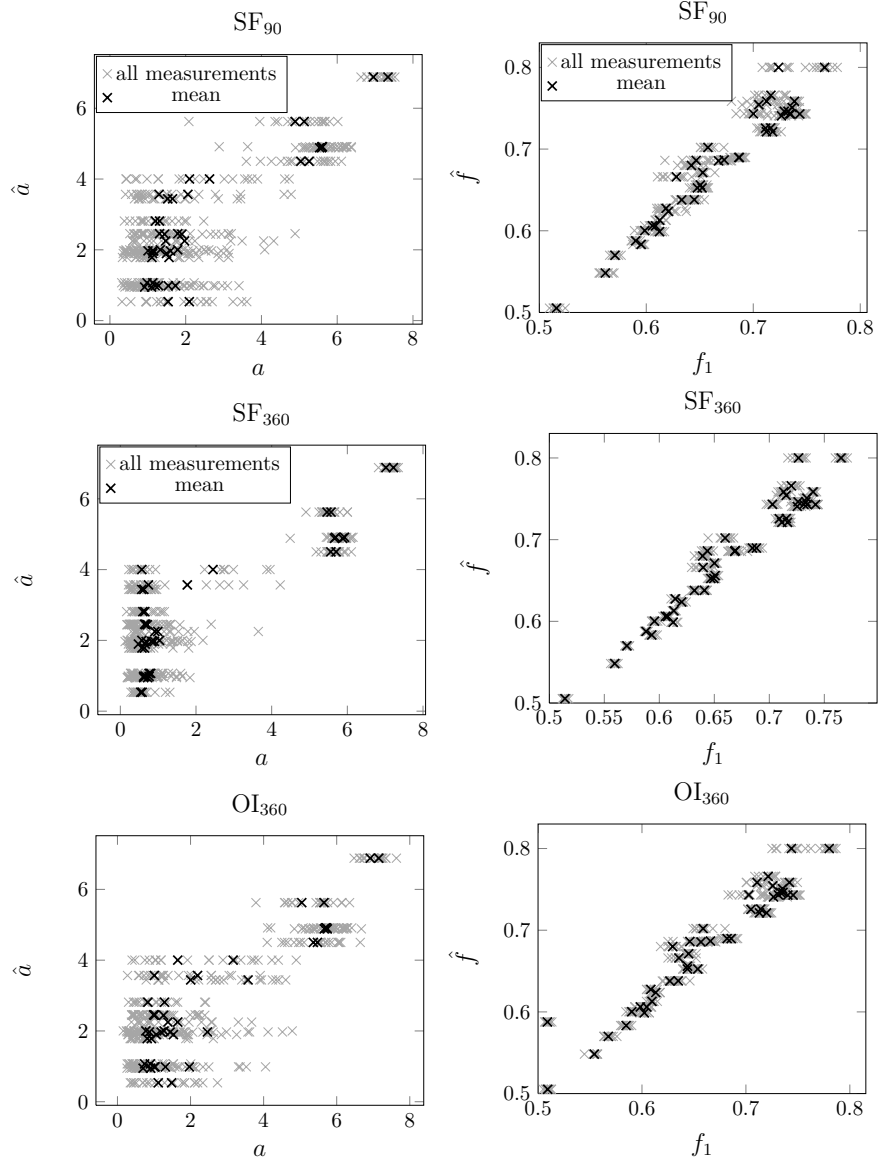
Figure 1.2: Scatter plots of estimated tissue model parameters a and f_1 (grey) and and mean a and f_1 over 10 replications (black) against true $\hat{a}$ and $\hat{f}$ of the MC substrates.
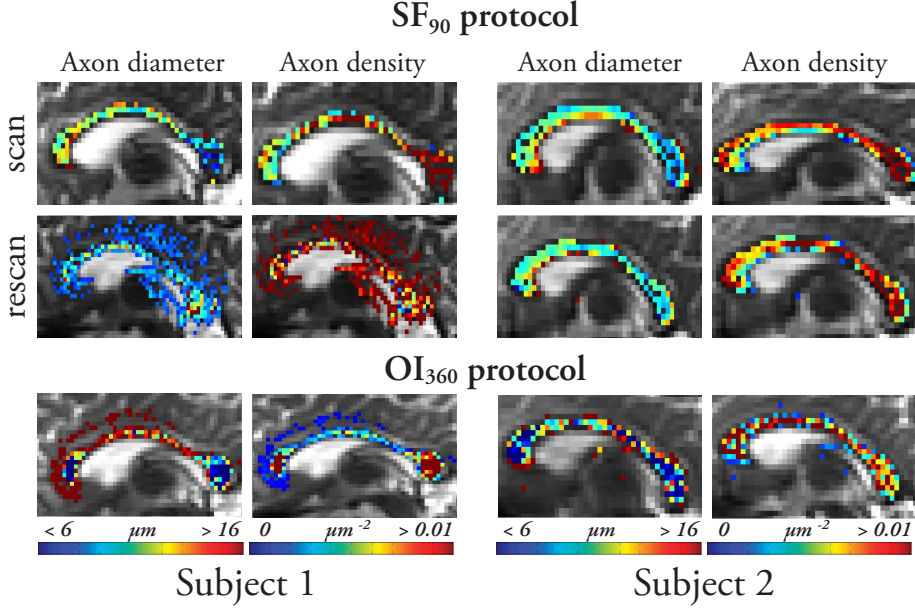
Figure 1.3: Color coded parameter maps of a and ρ in the centre slice of the CC in two subjects. Scan and rescan results for the $\mathcal{SF}_{90}$ are shown together with results from the $\mathcal{OI}_{360}$ acquisition.

MRI experiment

Figure 1.3 shows maps of a and ρ in the centre slice of the CC for all acquisitions in two volunteers. From previous histological studies **?** we expected low axon diameter and high density in the splenium and genu and higher axon diameters with lower density in the body of the CC. As predicted by the MC simulations (see also Alexander et al. (2010)), all protocols overestimated a because of the lack of sensitivity to lower diameters. The high-low-high trend in a and low-high-low trend of ρ can be observed in both subjects in $\mathcal{OI}_{360}$ results but are less apparent in $\mathcal{SF}_{90}$ scans. The worst case is is $\mathcal{SF}_{90}$ of subject 1, which presents very noisy parameter maps. This is likely to be caused by a misalignment with the true fibre direction of the CC and the gradient directions, which demonstrates the sensitivity of the SF protocol to accurate positioning. Furthermore, all SF scans consistently produce larger estimates of a than $\mathcal{OI}_{360}$. Variation in true fibre orientation is again the likely explanation. Unlike the SF protocols, the OI protocol can better compensate for this variation because of the high angular gradient sampling. However, despite the limitations, the results of subject 2 demonstrate reproducible estimates of a and ρ. This suggests that with accurate positioning, the 20 minute $\mathcal{SF}_{90}$ protocol is able to produce comparable parameter maps to $\mathcal{OI}_{360}$, which requires more than three times the scan time.

protocol visualisation

1.5   Discussion

In this work we propose optimised Diffusion Weighted Imaging (DWI) protocols that use the known fibre orientation in specific structures like the CC and allow us to estimate indices of axon diameter and density in the live human brain. We develop a new optimization algorithm that overcomes several limitations of previous approaches and produces DWI protocols that can be acquired in under 20 minutes. While previous protocols were too time consuming for clinical practise, the short acquisition time of our protocols opens the possibility to be included in a variety of studies. Experiments on synthetic data show that our protocols can provide axon diameter and density indices with similar variance to those from longer orientational invariant protocols. In-vivo scans on two healthy volunteers show the potential of our method to produce parameter maps of axon diameter and density that agree with the general histologic trend but also reveal the limitations caused by misalignment and variation in fibre orientation compared to the longer OI protocol. If such protocols are to be used, great care must be taken to align gradient directions with the fibre orientation. Future work aims to account for uncertain or erroneous fibre orientation by incorporating some tolerance for fibre orientation variation in the optimisation.

Bibliography

Alexander, D. C. (2008). A general framework for experiment design in diffusion MRI and its application in measuring direct tissue-microstructure features. *Magnetic Resonance in Medicine*, *60*(2), 439–448.

Alexander, D. C., Hubbard, P. L., Hall, M. G., Moore, E. A., Ptito, M., Parker, G. J. M., & Dyrby, T. B. (2010). Orientationally invariant indices of axon diameter and density from diffusion MRI. *NeuroImage*.

Assaf, Y., Blumenfeld-Katzir, T., Yovel, Y., & Basser, P. J. (2008). AxCaliber: a method for measuring axon diameter distribution from diffusion MRI. *Magnetic Resonance in Medicine*, *59*(6), 1347–1354.

Avram, L., Ã-zarslan, E., Assaf, Y., Bar-Shir, A., Cohen, Y., & Basser, P. J. (2008). Three-dimensional water diffusion in impermeable cylindrical tubes: theory versus experiments. *NMR Biomed.*, *21*(8), 888–898.
URL `http://dx.doi.org/10.1002/nbm.1277`

Barazany, D., Basser, P. J., & Assaf, Y. (2009). In vivo measurement of axon diameter distribution in the corpus callosum of rat brain. *Brain*.

Cook, P. A., Symms, M., Boulby, P. A., & Alexander, D. C. (2007). Optimal acquisition orders of diffusion-weighted MRI measurements. *Journal of Magnetic Resonance Imaging*, *25*(5), 1051–1058.
URL `http://dx.doi.org/10.1002/jmri.20905`

Golabchi, F. N., Brooks, D. H., Hoge, W. S., Girolami, U. D., & Maier, S. E. (2010). Pixel-based comparison of spinal cord MR diffusion anisotropy with axon packing parameters. *Magn Reson Med*, *63*(6), 1510–1519.

Panagiotaki, E., Schneider, T., Siow, B., Hall, M. G., Lythgoe, M. F., & Alexander, D. C. (2012). Compartment models of the diffusion mr signal in brain white matter: A taxonomy and comparison. *NeuroImage*, *59*(3), 2241–2254.
URL `http://www.sciencedirect.com/science/article/pii/S1053811911011566`

Siow, B., Drobnjak, I., Chatterjee, A., Lythgoe, M. F., & Alexander, D. C. (2012). Estimation of pore size in a microstructure phantom using the optimised gradient waveform diffusion weighted nmr sequence. *Journal of Magnetic Resonance*, *214*(0), 51–60.
URL `http://www.sciencedirect.com/science/article/pii/S1090780711003806`

Stanisz, G. J., Wright, G. A., Henkelman, R. M., & Szafer, A. (1997). An analytical model of restricted diffusion in bovine optic nerve. *Magnetic Resonance in Medicine*, *37*(1), 103–111.
URL `http://onlinelibrary.wiley.com/doi/10.1002/mrm.1910370115/abstract`

Stejskal, E. O., & Tanner, J. E. (1965). Spin Diffusion Measurements: Spin Echoes in the Presence of a Time-Dependent Field Gradient. *Journal of Chemical Physics*, *42*, 288.

Szafer, A., Zhong, J., & Gore, J. C. (1995). Theoretical model for water diffusion in tissues. *Magnetic Resonance in Medicine*, *33*(5), 697–712.
URL `http://onlinelibrary.wiley.com/doi/10.1002/mrm.1910330516/abstract`

Wang, Y., Wang, Q., Haldar, J. P., Yeh, F.-C., Xie, M., Sun, P., Tu, T.-W., Trinkaus, K., Klein, R. S., Cross, A. H., & Song, S.-K. (2011). Quantification of increased cellularity during inflammatory demyelination. *Brain*, *134*(12), 3590–3601.
URL `http://brain.oxfordjournals.org/content/134/12/3590`

Zhang, H., Hubbard, P. L., Parker, G. J., & Alexander, D. C. (2011). Axon diameter mapping in the presence of orientation dispersion with diffusion mri. *NeuroImage*, *56*(3), 1301–1315.
URL   `http://www.sciencedirect.com/science/article/pii/S1053811911001376`